



HAL
open science

Unravelling the postural diversity of mammals: Contribution of humeral cross-sections to palaeobiological inferences

Jordan Gônet, Jérémie Bardin, Marc Girondot, John R Hutchinson, Michel
Laurin

► **To cite this version:**

Jordan Gônet, Jérémie Bardin, Marc Girondot, John R Hutchinson, Michel Laurin. Unravelling the postural diversity of mammals: Contribution of humeral cross-sections to palaeobiological inferences. *Journal of Mammalian Evolution*, inPress, 10.1007/s10914-023-09652-w . hal-03996717

HAL Id: hal-03996717

<https://hal.science/hal-03996717>

Submitted on 8 Mar 2023

HAL is a multi-disciplinary open access archive for the deposit and dissemination of scientific research documents, whether they are published or not. The documents may come from teaching and research institutions in France or abroad, or from public or private research centers.

L'archive ouverte pluridisciplinaire **HAL**, est destinée au dépôt et à la diffusion de documents scientifiques de niveau recherche, publiés ou non, émanant des établissements d'enseignement et de recherche français ou étrangers, des laboratoires publics ou privés.

1 **Unravelling the postural diversity of mammals:**
2 **Contribution of humeral cross-sections to palaeobiological**
3 **inferences**

4 Jordan Gônet^{1*} · Jérémie Bardin¹ · Marc Girondot² · John R. Hutchinson³ · Michel Laurin¹

5
6 ¹Centre de recherche en paléontologie – Paris, UMR 7207, Sorbonne Université, Muséum
7 national d’histoire naturelle, Centre national de la recherche scientifique, 8 rue Buffon, 75005
8 Paris, France

9 ²Laboratoire écologie, systématique et évolution, UMR 8079, AgroParisTech, Université Paris-
10 Saclay, Centre national de la recherche scientifique, 91405 Orsay, France

11 ³Structure and Motion Laboratory, Department of Comparative Biomedical Sciences, Royal
12 Veterinary College, AL9 7TA Hatfield, UK

13 *Corresponding author: jordan.gonet@edu.mnhn.fr

14
15 Keywords: Functional morphology · Humerus · Limb posture · Mammal · Microanatomy ·
16 Palaeobiology

17 **Abstract**

18 Mammals have an evolutionary history spanning hundreds of millions of years. Today,
19 mammals represent one of the most diverse groups of tetrapod vertebrates. In particular, they
20 present a great postural diversity. The humerus adopts different positions: small mammals have
21 a “crouched” posture with a quasi-horizontal humerus, while in the largest species, the humerus
22 is more vertical. Some monotremes have more transversely oriented humeri similar to those of
23 reptiles. The forelimb of moles is also modified in relation to their burrowing lifestyle. This
24 postural diversity is accompanied by an important microanatomical disparity. Indeed, the bones
25 of the appendicular skeleton support the weight of the body and are subjected to various forces
26 that partly shape their external and internal morphology. We show here how geometric and
27 microanatomical parameters measured in cross-section such as the polar section modulus or the
28 position of the medullo-cortical transition can be related to posture. Using statistical methods
29 that take phylogeny into account, we develop a postural model from a sample of humerus cross-
30 sections belonging to 41 species of extant mammals. Our model can be used by palaeontologists
31 to infer the posture of extinct synapsids. As an example, we infer the posture of two emblematic
32 taxa: *Dimetrodon natalis* and *Peratherium cuvieri*. The results of the analysis indicate a
33 sprawling posture for *Dimetrodon* and a crouched posture for *Peratherium*. This work
34 contributes to unravel the complex interaction between phylogeny, humeral microanatomy and
35 geometry, body mass, lifestyle and posture in mammals.

36 **Introduction**

37 Mammals are a highly successful group of tetrapod vertebrates with a long evolutionary history.
38 Their earliest stem members, i.e. the first synapsids (the term “stem mammal” is used
39 throughout this study to refer to any taxon that is more closely related to Mammalia than to
40 Reptilia but that does not belong to the mammalian crown group), originated in the
41 Carboniferous, about 330 million years ago, with the emergence of the first amniotes (Didier
42 and Laurin 2020), and have undergone several episodes of diversification ever since. The Late
43 Carboniferous and Early Permian is dominated by eupelycosaurs. These are followed by
44 therapsids by the middle Permian; they comprised medium-sized herbivorous and carnivorous
45 taxa that became extinct by the end of the Triassic, except for cynodonts, which gave rise to the
46 Mammaliaformes during the Triassic (Kemp 2005; Brocklehurst et al. 2013). It is generally
47 thought that most Mesozoic mammals were small, nocturnal creatures with more or less
48 burrowing habits and a generalised insectivory (Jenkins and Parrington 1976; Kielan-
49 Jaworowska et al. 2004; Gerkema et al. 2013; but see Hu et al. 2005; Gill et al. 2014; Meng
50 2014; Debuyschere 2015). The K-Pg extinction event was the starting point for the Cenozoic
51 radiation of mammals which led them to colonise the ecological niches left empty by non-avian
52 dinosaurs (Rose 2006; but see Wilson et al. 2012). Today, mammals are extremely diverse, both
53 taxonomically and ecologically. With over 5,000 currently recognised extant species (Upham
54 et al. 2019), they are found all over the world, at all levels of the trophic network, on land, in
55 the seas and in the air (Vaughan et al. 2015). They range in size from the bumblebee bat, which
56 weighs only a few grams, to the blue whale (the largest animal on the planet), which weighs
57 more than 100 tons, the weight of a few dozen elephants. Mammals are also particularly diverse
58 in their posture: small mammals like rodents have a “crouched” posture, with a quasi-horizontal
59 humerus (Jenkins 1971), while in the cursorial and graviportal taxa, such as artiodactyls and
60 proboscideans, the humerus is more vertical (Gregory 1912). Some monotremes have more
61 transversely oriented humeri (Pridmore 1985). The forelimb of moles is also modified in
62 relation to their burrowing lifestyle (Lin et al. 2019).

63 The shape of biological structures is determined by at least three types of constraints
64 that can be positioned at the three vertices of an abstract triangle in the framework of
65 constructional morphology (Seilacher 1970). These are phylogenetic (heredity), structural
66 (development), and adaptive (function) constraints. The bones of the appendicular skeleton are
67 subject to these different constraints, especially functional constraints relative to posture.
68 Indeed, limb bones support the weight of the body and are affected by various forces that partly

69 shape their external and internal morphology. While many studies have already identified the
70 link between lifestyle (from aquatic to terrestrial) and bone microanatomy, including using
71 multivariate quantitative methods that take phylogeny into account (Germain and Laurin 2005;
72 Krilloff et al. 2008; Canoville and Laurin 2009, 2010; Laurin et al. 2011; Quemeneur et al. 2013;
73 Amson et al. 2014; Ibrahim et al. 2014; Nakajima et al. 2014; Cooper et al. 2016; Houssaye et
74 al. 2016a; Klein et al. 2016; Houssaye and Botton-Divet 2018; Kilbourne and Hutchinson 2019;
75 Canoville et al. 2021; Fabbri et al. 2022), fewer have attempted to link the geometric and
76 microanatomical properties of limb bones to posture (Houssaye et al. 2016b; Bishop et al.
77 2018a, 2018b, 2018c; Plasse et al. 2019; Main et al. 2021; Wagstaffe et al. 2022).

78 Although it is accepted that mammals, like reptiles such as dinosaurs and
79 pseudosuchians (Hutchinson 2006), experienced a postural transition from approximately
80 transversely-oriented to more parasagittally-oriented limbs, the timing of this transition has
81 been widely debated without reaching a consensus. Some authors (Jenkins 1973; Pridmore
82 1985; Sereno 2006) have argued that early mammals had already acquired a parasagittal limb
83 posture and gait by the Late Triassic/Early Jurassic, while others (Gambaryan and Kielan-
84 Jaworowska 1997; Kielan-Jaworowska and Hurum 2006) favoured the hypothesis of a later
85 acquisition in early therians. Even today, posture in mammals and in older stem taxa such as
86 *Dimetrodon*, raises many questions that triggered numerous studies that enrich our knowledge
87 of the evolution of locomotion in mammals (Abbott 2019; Regnault et al. 2020; Jones et al.
88 2021; Brocklehurst et al. 2022).

89 Our study is a logical extension of these works. Using generalised least squares, we
90 investigate the relationship between humeral posture and geometric and microanatomical data
91 collected from humeral bone cross-sections belonging to 41 extant mammalian species, while
92 taking phylogeny into account. Body mass and lifestyle were also included in our models as
93 both are known to be related to posture and/or bone microanatomy, e.g. large taxa tend to have
94 greater bone compactness and more upright limbs (Biewener 1989b; Houssaye et al. 2016b);
95 fossorial talpids have greater extension of the medullo-cortical transition compared to terrestrial
96 talpids (Meier et al. 2013). We use the collected data to generate a phylogenetically informed
97 postural inference model capable of generating postural predictions in extinct taxa. We apply
98 the model to two taxa: *Dimetrodon natalis* (a small *Dimetrodon* species) and *Peratherium*
99 *cuvieri* (“Cuvier’s Sarigue”). While *Dimetrodon* is a stem mammal, *Peratherium* is a putative
100 marsupialiform. *Dimetrodon* and *Peratherium* lived in the Early Permian and Late Eocene,
101 respectively, well before and well after the Mesozoic postural transition in mammals. The

102 posture of *Dimetrodon* has been extensively studied since its discovery in the second half of the
103 19th century. The recent interpretation indicates a more or less sprawling posture. In
104 comparison, *Peratherium* has been the subject of less work, but its younger geological age and
105 general anatomy are compatible with a more crouched posture. These two taxa are therefore
106 perfect candidates to test our method.

107 **Materials and Methods**

108 BIOLOGICAL SAMPLE

109 To train our statistical model, we compiled a set of geometric and microanatomical data
110 collected on humeral mid-diaphyseal cross-sections from a large number of mammalian taxa
111 with a known posture. The dataset included 43 individuals from 41 extant species (Table 1;
112 Online Resource 1). We built our dataset to be as taxonomically exhaustive as possible and to
113 maximise coverage of the postural diversity of Mammalia. We used our postural models to infer
114 the posture of two extinct taxa of interest: the Early Permian stem mammal *Dimetrodon natalis*
115 (IPBSH-4) and the Late Eocene herpetotheriid *Peratherium cuvieri* (MNHN-F-GY679b); see
116 Online Resource 1.

117 POSTURAL DEFINITIONS

118 Most non-flying mammals are obligate quadrupeds, that is, they move exclusively on four limbs
119 (Vaughan et al. 2015). A few taxa, especially among rodents, marsupials and primates, are
120 known to be facultatively bipedal or quadrupedal, meaning that they alternate between
121 bipedalism and quadrupedalism (D'Août et al. 2004; Russo and Kirk 2017). Some pangolins
122 (*Smutsia temminckii*) are also able to move on their hind limbs for some distance (Pietersen et
123 al. 2020). Obligate bipedalism is restricted to humans (Niemitz 2010).

124 Yet, mammals show great diversity in limb posture, especially regarding the humerus
125 (Fig. 1). During normal walking, the specialised “erect” (or upright) forelimb posture of
126 mammals exhibits fairly low humeral abduction (less than 10 degrees to the parasagittal plane;
127 Jenkins 1971). The humerus is oblique with the elbow always functioning below the shoulder
128 joint between approximately 30 and 75 degrees from the horizontal. Erect limbs are found in
129 “hoofed” mammals such as artiodactyls and proboscideans (Gregory 1912), in carnivorans
130 (Blob 2000) and in cursorial and graviportal mammals in general (Gregory 1912; Jenkins 1971;
131 but see Stein and Casinos 1997; Carrano 1999). Taxa with more generalised locomotor
132 adaptations, such as rodents, have a so-called “crouched” posture (Jenkins 1971). The humerus

133 **Table 1** List of the mammalian taxa included in this study. Taxa are presented in alphabetical
 134 order. Body mass is rounded to the nearest gram. *Data collected on
 135 <https://www.morphosource.org>. Abbreviations: Aq, semi-aquatic; Ar, arboreal; C, crouched; E,
 136 erect; Fo, fossorial; M, modified; S, sprawling; Te, terrestrial. Institutional abbreviations:
 137 IPBSH/STIPB, Steinmann-Institut, Universität Bonn, Germany; MNHN, Muséum national
 138 d'Histoire naturelle, Paris, France; NHMUK, Natural History Museum, London, United
 139 Kingdom; UFGK, Ur- und Frühgeschichte Köln, Cologne, Germany; UMZC, Cambridge
 140 University Museum of Zoology, Cambridge, United Kingdom

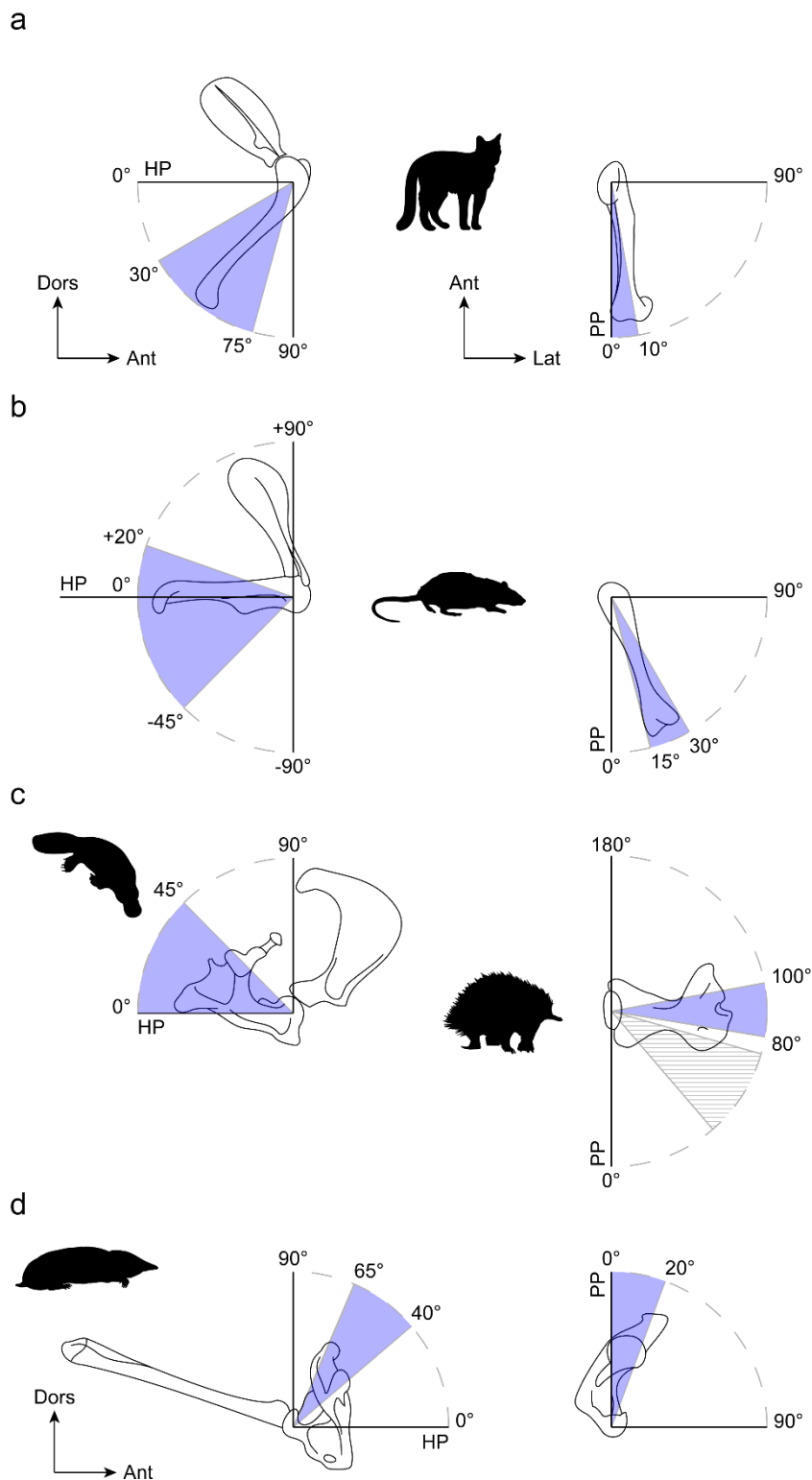
Taxon		Collection number	Humeral posture	Lifestyle	Body mass (g)	
Afrosoricida	Chrysochloridae	<i>Chrysochloris asiatica</i>	MNHN-ZM-MO-1991-626	C	Fo	37
Artiodactyla	Bovidae	<i>Cephalophus silvicultor</i>	NHMUK ZD 1961.8.9.80-1	E	Te	62,007
		<i>Rupicapra rupicapra</i>	STIPB M1639	E	Te	35,383
		<i>Syncerus caffer</i>	NHMUK ZD 1874.11.2.4	E	Te	646,333
	Cervidae	<i>Alces americanus</i>	UMZC H.17,691	E	Te	368,500
		<i>Cervus elaphus</i>	MNHN unnumbered specimen	E	Te	160,167
		<i>Rangifer tarandus</i>	STIPB M47	E	Te	101,250
	Suidae	<i>Sus scrofa</i>	MNHN unnumbered specimen	E	Te	135,000
		<i>Sus scrofa</i>	STIPB M56	E	Te	135,000
Carnivora	Canidae	<i>Vulpes vulpes</i>	STIPB M12	E	Te	4,580
	Felidae	<i>Felis silvestris</i>	UFGK unnumbered specimen	E	Te	5,037
		<i>Panthera leo</i>	MNHN-ZM-AC-1912-398	E	Te	149,062
	Mustelidae	<i>Martes martes</i>	STIPB unnumbered specimen	C	Ar	1,300
		<i>Mustela putorius</i>	STIPB unnumbered specimen	C	Te	809
	Ursidae	<i>Ursus americanus</i>	MNHN-ZM-MO-1902-1415	E	Te	132,405
Cingulata	Dasypodidae	<i>Dasypus novemcinctus</i>	MNHN-ZM-MO-2001-1317	C	Te	3,949
Diprotodontia	Macropodidae	<i>Macropus giganteus</i>	MNHN-ZM-AC-A10098	C	Te	41,455
		<i>Thylogale stigmatica</i>	umzc:vertebrates:a12.44/1*	C	Te	4,306
	Potoroidae	<i>Aepyprymnus rufescens</i>	msu:mr:mr.4680*	C	Fo	2,820
	Vombatidae	<i>Vombatus ursinus</i>	MNHN-ZM-AC-A3289	C	Fo	25,750
Eulipotyphla	Erinaceidae	<i>Erinaceus europaeus</i>	STIPB unnumbered specimen	C	Te	778

	Solenodontidae	<i>Solenodon paradoxus</i>	MNHN-ZM-MO-1980-237	C	Fo	900
	Talpidae	<i>Euroscaptor micrura</i>	MNHN-ZM-MO-1959-1795	M	Fo	60
		<i>Talpa europaea</i>	MNHN-ZM-MO-1953-829	M	Fo	110
		<i>Talpa europaea</i>	STIPB unnumbered specimen	M	Fo	110
Monotremata	Ornithorhynchidae	<i>Ornithorhynchus anatinus</i>	MNHN-ZM-AC-1906-484	S	Aq	1,225
	Tachyglossidae	<i>Tachyglossus aculeatus</i>	MNHN-ZM-AC-1884-1125	S	Fo	3,170
Pholidota	Manidae	<i>Smutsia temminckii</i>	MNHN-ZM-AC-1897-134	C	Te	9,587
Primates	Cercopithecidae	<i>Chlorocebus aethiops</i>	MNHN-ZM-AC-1909-262	E	Ar	5,104
		<i>Macaca radiata</i>	MNHN-ZM-AC-1845-271	E	Ar	5,132
	Hominidae	<i>Pan paniscus</i>	amnh:mammals:m-202870*	E	Ar	35,120
	Lemuridae	<i>Lemur catta</i>	MNHN-ZM-AC-1910-101	C	Ar	2,555
Rodentia	Dipodidae	<i>Allactaga elater</i>	UF:mammal:30045*	C	Fo	59
		<i>Dipodomys ordii</i>	MNHN-ZM-MO-1958-294	C	Fo	50
		<i>Zapus princeps</i>	uwbm:mammal specimens:74482*	C	Te	28
		<i>Zapus trinotatus</i>	uwbm:mammal specimens:OG-7813*	C	Te	27
	Hystriidae	<i>Hystrix cristata</i>	MNHN-ZM-AC-1922-386	C	Fo	19,167
	Muridae	<i>Gerbillus campestris</i>	MNHN-ZM-MO-1990-10	C	Fo	28
		<i>Meriones libycus</i>	MNHN-ZM-MO-1981-619	C	Fo	91
	Pedetidae	<i>Pedetes capensis</i>	MNHN-ZM-AC-1883-1640	C	Fo	2,775
	Sciuridae	<i>Marmota marmota</i>	STIPB unnumbered specimen	C	Fo	3,500
Scandentia	Tupaiaidae	<i>Tupaia belangeri</i>	STIPB unnumbered specimen	C	Ar	200
Tubulidentata	Orycteropodidae	<i>Orycteropus afer</i>	MNHN-ZM-AC-1919-19	C	Fo	56,175

141

142 is more abducted than in erect mammals (between 15 and 30 degrees relative to the parasagittal
143 plane; Jenkins 1971); and the humerus is also more horizontal, with the elbow oscillating from
144 about 20 degrees above the shoulder joint to 45 degrees below it. Both erect and crouched taxa
145 belong to the same morpho-functional continuum, with graviportal and cursorial taxa
146 representing the two extreme morphologies (Carrano 1999).

147 Besides this general pattern, some taxa have atypical humeral postures. The monotremes
148 *Tachyglossus* and *Ornithorhynchus* have more “sprawling” humeri, akin to what exists in extant



149 **Fig. 1** Humeral excursion at the shoulder joint in lateral (left) and dorsal (right) views in several
 150 mammals with different postures (Jenkins 1971; Pridmore 1985; Lin et al. 2019). The scapula
 151 and humerus are shown in lateral view, but the scapula is not shown in dorsal view for better
 152 visibility of the humerus. a. erect humerus in *Felis domestica*; b. crouched humerus in *Rattus*
 153 *norvegicus*; c. sprawling humerus in *Ornithorhynchus* (left and hatched area on right) and

154 *Tachyglossus* (right); d. modified humerus in *Scalopus aquaticus*. Abbreviations: HP,
155 horizontal plane; PP, parasagittal plane. Silhouettes come from phylopic.org

156 ectothermic reptiles (Bakker 1971; but see Pridmore 1985; Gambaryan and Kuznetsov 2013).
157 In *Tachyglossus*, the humerus is completely horizontal. The elbow oscillates laterally between
158 80 and 100 degrees from the parasagittal plane (Jenkins 1971; Pridmore 1985). In
159 *Ornithorhynchus*, the humerus is abducted between 40 and 75 degrees from the parasagittal
160 plane, with the elbow operating above the shoulder joint up to 45 degrees from the horizontal
161 (Pridmore 1985). The forelimb of moles (Talpidae) is also highly modified in relation to their
162 burrowing behaviour. The humerus is slightly abducted (less than 20 degrees from the
163 parasagittal plane). The elbow oscillates cranially relative to the shoulder joint, rising 40 to 65
164 degrees from the horizontal plane (Lin et al. 2019).

165 DATA ACQUISITION

166 We measured various geometric and microanatomical parameters that have been previously
167 associated in the literature with locomotion and posture, and more generally with lifestyle in
168 amniotes (Canoville and Laurin 2009, 2010; Amson et al. 2014; Houssaye et al. 2016b;
169 Houssaye and Botton-Divet 2018; Scheidt et al. 2019). This was done on cross-sections of
170 mammalian humeral shafts obtained mainly from CT data retrieved from the literature and from
171 morphosource.org. We scanned some of the specimens on the AST-RX platform of the Muséum
172 national d'histoire naturelle and on the MRI platform of the Université de Montpellier. We
173 extracted a cross-section from the CT data where the perimeter of the shaft was the smallest
174 because this is an area where mechanical stresses generally are important (Beck et al. 1996;
175 Tommasini et al. 2005; Campione and Evans 2012), resulting in more or less mid-diaphyseal
176 cross-sections. We also incorporated into our data mid-diaphyseal traditional histological
177 sections (unpublished data from Quemeneur et al. 2013). Mixing sections with slightly different
178 reference planes in comparative studies is not considered a problem as long as the species of
179 interest does not show excessive longitudinal microanatomical variation (Amson and Kolb
180 2016; Houssaye et al. 2018). The scans were processed in ImageJ (Abràmoff et al. 2004) and
181 MorphoDig (Lebrun 2018). Each bone was oriented so that the section plane was as
182 perpendicular as possible to the long axis of the diaphysis. Data for all left humeri were
183 symmetrised so that the sample consisted of right side bones only. We binarised the cross-
184 sections before taking our geometric and microanatomical measurements in ImageJ with the
185 BoneJ plugin (Doube et al. 2010) and in R (R Core Team 2013) with the BoneProfileR package

186 (Girondot and Laurin 2003; Gônet et al. 2022). A sample of the mammalian cross-sections used
187 in this study are presented in Fig. 2.

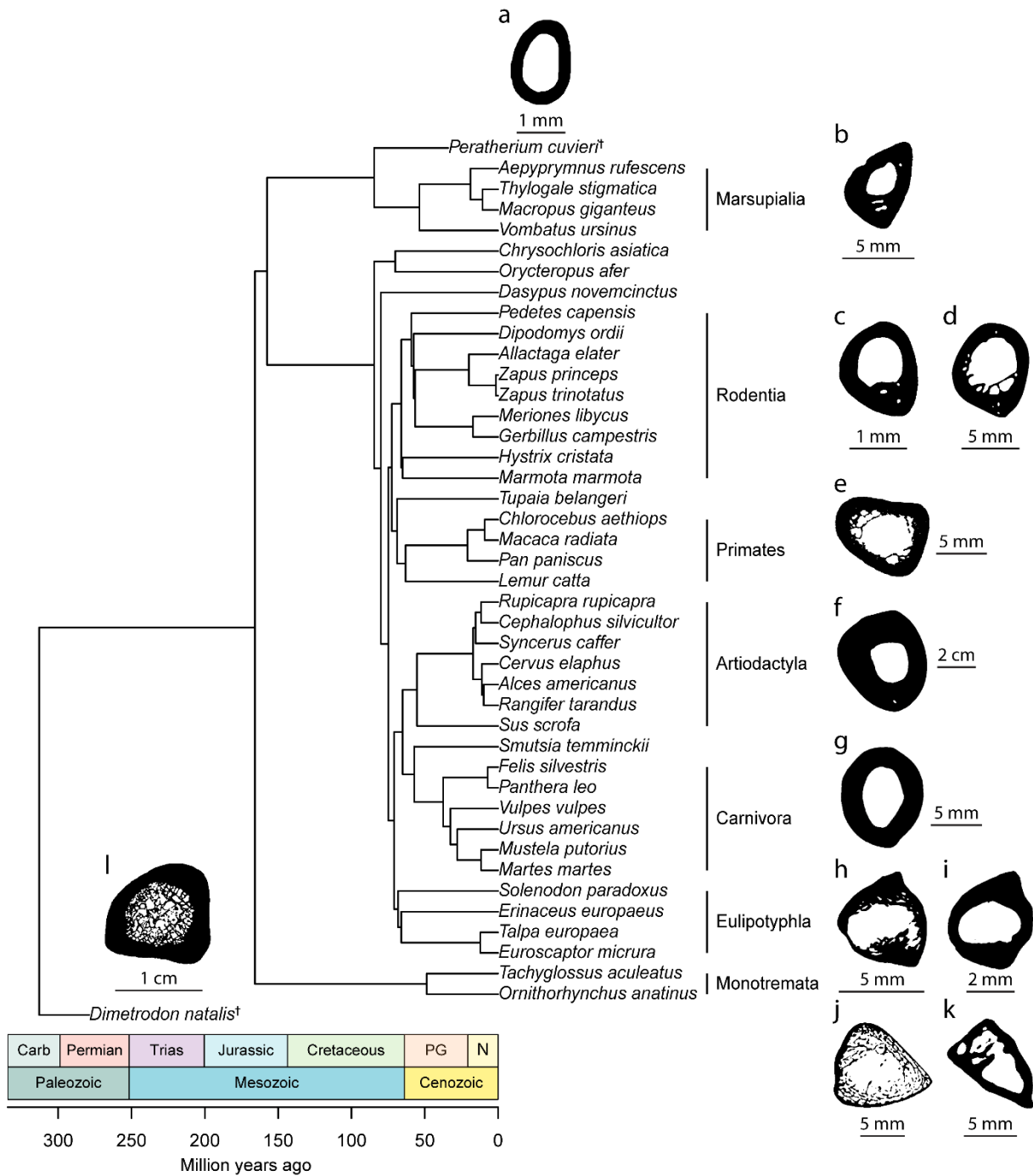
188 We measured six geometric parameters with BoneJ (Fig. 3): P_{\min} , the minimum
189 perimeter of the shaft; BCSA, the area occupied by the bone on the section; TCSA, the total
190 area of the section; Ecc, the eccentricity of the section corresponding to the ratio of the area
191 moments of inertia (I) around the major and minor axes (I_{\max}/I_{\min}); SR, the slenderness ratio (a
192 high SR indicates a slender bone, while a low SR indicates a more robust bone; see Eq. 1); Z_{pol} ,
193 the polar section modulus reflecting the resistance of the shaft to torsion (the higher Z_{pol} , the
194 more resistant the bone will be to torsion). Although Z_{pol} can be used with subcircular cross-
195 sections, which is the case for most taxa, it is ideally used with circular cross-sections.

196
$$\text{Slenderness ratio} = \frac{\text{Bone length}}{\sqrt{\frac{I_{\min}}{\text{TCSA}}}} \quad (1)$$

197 We used BoneProfileR to measure seven microanatomical parameters (Fig. 3). We set
198 BoneProfileR to determine the position of the centre of unmineralisation, i.e. the centre of the
199 unmineralised spaces in the bone section, and segment the cross-section into 100 concentric
200 circles. Bone compactness (measured by the number of bone pixels relative to the total number
201 of pixels) was measured in each circle from the centre of the medulla to the edge of the cross-
202 section. We extracted several parameters from the resulting compactness profiles: P, the
203 distance of the medullo-cortical transition from the centre of the cross-section (a high P
204 generally reflects low bone compactness); S, the inverse of the asymptote of the slope at point
205 P (a high S corresponds to a gradual transition between the medulla and the cortex, as in the
206 case of cancellous bone, while a low S reflects an abrupt transition). BoneProfileR also
207 computes an observed global compactness value, C_{obs} . In addition, we performed a radial
208 analysis to extract the radial component of the parameters P and S: the cross-section is
209 segmented into 60 slices of 6 degrees and a compactness profile is drawn for each slice. The
210 radial component of P (RP) and S (RS) is the average of the P and S of all slices. The standard
211 deviation associated with RP and RS is RPSD and RSSD, respectively. When a species in our
212 sample was represented by more than one individual, we calculated the mean value for each
213 microanatomical parameter.

214 BUILDING REFERENCE PHYLOGENIES

215 We constructed a set of 100 reference trees of mammals to include phylogenetic uncertainty in
216 our statistical analyses (Fig. 2). The trees were manipulated in R using the packages phytools



217 **Fig. 2** Tree 1 of our set of 100 time-calibrated composite phylogenies displaying the
 218 evolutionary relationships among the extant and extinct species included in this study, with
 219 some of the humeral cross-sections analysed. a. *Peratherium cuvieri*† (Late Eocene) MNHN-
 220 F-GY679b (unknown); b. *Aepyprymnus rufescens* MorphoSource: msu:mr:mr.4680
 221 (crouched); c. *Meriones libycus* MNHN-ZM-MO-1981-619 (crouched); d. *Marmota marmota*
 222 STIPB unnumbered specimen (crouched); e. *Macaca radiata* MNHN-ZM-AC-1845-271
 223 (crouched); f. *Syncerus caffer* NHMUK ZD 1874.11.2.4 (erect); g. *Felis silvestris* UFGK
 224 unnumbered specimen (erect); h. *Talpa europaea* MNHN-ZM-MO-1953-829 (modified); i.
 225 *Euroscaptor micrura* MNHN-ZM-MO-1959-1795 (modified); j. *Tachyglossus aculeatus*

226 MNHN-ZM-AC-1884-1125 (sprawling); k. *Ornithorhynchus anatinus* MNHN-ZM-AC-1906-
227 484 (sprawling); l. *Dimetrodon natalis*† (Early Permian) IPBSH-4 (unknown). The cross-
228 sections are anatomically oriented (anterior to the top and lateral to the right) except for
229 *Dimetrodon*. Trees were compiled in R using the work of Selva (2017), Upham et al. (2019),
230 and Didier and Laurin (2020)

231 (Revell 2012) and TreePar (Stadler 2011). We extracted 100 trees with only the species of
232 interest from a distribution of 10 000 Bayesian supertrees of mammals calibrated in time (node-
233 dating, 5911 species) from the publication of Upham et al. (2019) and available on vertlife.org.
234 The statistical analyses in this study required reference trees that included the taxa for which
235 we wanted to infer posture. Therefore, *Dimetrodon natalis* (Sphenacodontidae) was branched
236 at 313 Ma based on Didier and Laurin (2020). We followed Selva (2017) in considering
237 *Peratherium cuvieri* an herpetotheriid and set the age of divergence between Herpetotheriidae
238 and Marsupialia at approximately 85 Ma. The trees in Newick tree format are provided in
239 Online Resource 2

240 BODY MASS ESTIMATES AND LIFESTYLE

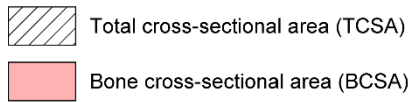
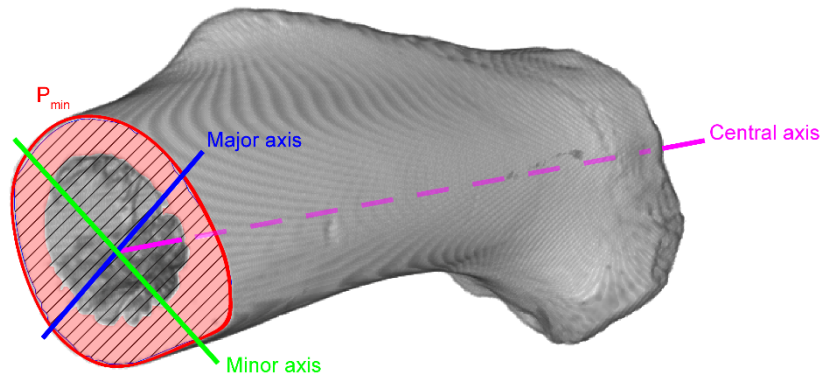
241 Body mass affects posture and bone microanatomy. Indeed, among mammals, the largest taxa
242 tend to have more erect/upright limbs and greater bone compactness (Biewener 1989b, 2005;
243 Hutchinson 2021). We therefore collected body mass estimates from the literature for each
244 taxon in our sample (Table 1; Online Resource 1). We relied entirely on the database of
245 Myhrvold et al. (2015), which compiles median body mass for a large number of extant
246 amniotes (we rounded values to the nearest gram).

247 Lifestyle is also known to be related to bone microanatomy, e.g., fossorial talpids have
248 greater extension of the medullo-cortical transition compared to terrestrial talpids (Meier et al.
249 2013). Thus, we defined four lifestyle categories based on limb use (semi-aquatic, terrestrial,
250 fossorial, and arboreal) to explore the potential relationship between lifestyle and posture (Table
251 1; Online Resource 1).

252 STATISTICAL TREATMENT IN A PHYLOGENETIC FRAMEWORK

253 *Phylogenetic signal*—We used the `phylosig` function from the R package `phytools` (Revell 2012)
254 to estimate the phylogenetic signal in each geometric and microanatomical parameters. The
255 `phylosig` function computes the K-statistic of Blomberg et al. (2003). A K-statistic greater than
256 1 indicates that closely related species in the tree show more similarity between them than what

Geometric parameters

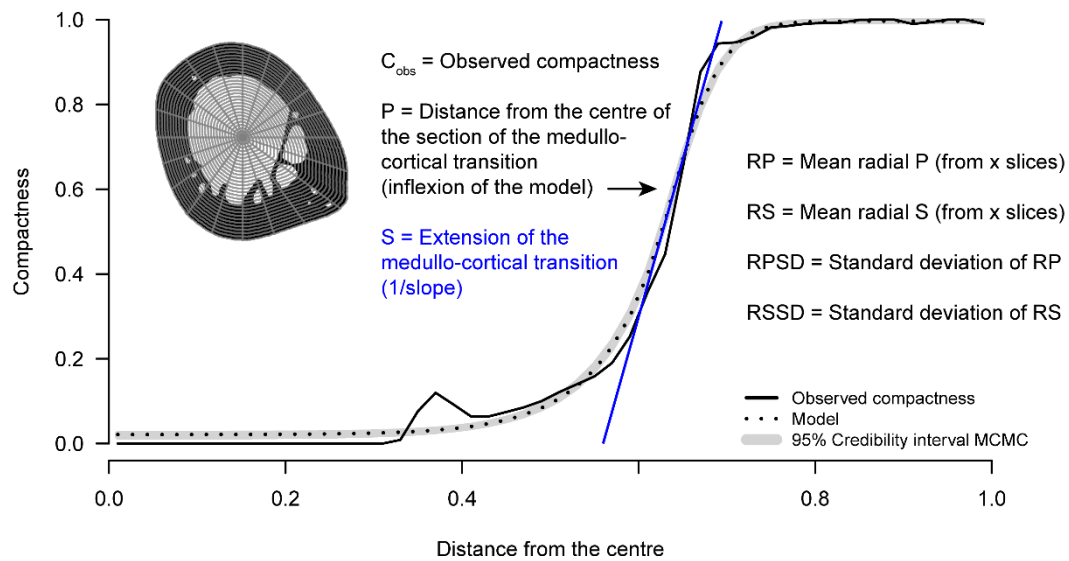


$$\text{Eccentricity (Ecc)} = \frac{\text{Area moment of inertia around the major axis } (I_{\max})}{\text{Area moment of inertia around the minor axis } (I_{\min})}$$

$$\text{Polar section modulus } (Z_{\text{pol}}) = \frac{\text{Polar moment of inertia (around the central axis)}}{\text{Radius of the cross-section}}$$

$$\text{Slenderness ratio (SR)} = \frac{\text{Bone length}}{\sqrt{\frac{I_{\min}}{\text{TCSA}}}}$$

Compactness parameters



257 **Fig. 3** All the geometric and compactness parameters measured in this study, illustrated here
 258 with a humerus of *Marmota marmota* (STIPB unnumbered specimen). The section on the
 259 compactness profile is divided into 30 concentric circles and 20 slices for better readability, but
 260 more were used in the analyses (100 and 60, respectively)

261 would be expected with a Brownian model of evolution, suggesting the existence of a
 262 substantial phylogenetic signal in the data. Conversely, a K-statistic lower than 1 implies that

263 closely related species are more different than expected highlighting evolutionary convergence
264 or higher variance between clades rather than within them.

265 We used the delta-statistic (Borges et al. 2019), which was designed for categorical
266 traits, to estimate the phylogenetic signal in posture. The delta-statistic depends on the
267 uncertainty associated with the inference of ancestral states: low uncertainty implies low
268 entropy (Shannon 1948) and a high delta-statistic. The higher the delta, the stronger the
269 phylogenetic signal.

270 A *P*-value is obtained by randomisation, i.e. a redistribution of the measured traits
271 among terminal branches. *K* and delta are computed 1000 and 100 times, respectively, with a
272 random distribution, then the pool of values obtained is compared to the *K* and delta with the
273 actual distribution. This was done for each tree in our phylogenetic tree sample.

274 *Generalised least squares*—We used the *gls* function from the R package nlme (Pinheiro et al.
275 2021) to model the relationship between each geometric and microanatomical parameter and
276 postural groups while accounting for phylogeny, body mass and lifestyle. The *gls* function fits
277 a linear model using least squares to optimise coefficients and allows a covariance structure to
278 be set between observations. Here, the expected covariance of a given trait (or a relationship
279 between traits) between two taxa corresponds to its evolution under a Brownian motion during
280 the time from the root to their last common ancestor.

281 *Phylogenetic flexible discriminant analysis*—We used phylogenetic flexible discriminant
282 analysis (PFDA) to explain posture in our sample of extant mammals and to predict humeral
283 posture in *Dimetrodon* and *Peratherium* based on geometric and microanatomical
284 measurements taken from humeral cross-sections while accounting for phylogeny. PFDA is a
285 classification model based on a combination of linear regressions. It is derived from flexible
286 discriminant analysis (FDA; Hastie et al. 1994) and corresponds to its phylogenetically
287 informed version (Motani and Schmitz 2011). In practice, PFDA corresponds to a *gls* where
288 categories are split in dummy variables and treated as continuous variables while phylogeny is
289 incorporated as a phylogenetic covariance matrix whose terms are multiplied by lambda to
290 make phylogenetic inertia variable through model optimisation (Pagel 1999). Lambda is
291 assigned a value between 0 and 1 that minimises the model error, that is, the share of variance
292 explained by phylogeny: 0 indicating that phylogeny does not explain the distribution of the
293 trait on the tree; 1 indicating that phylogeny explains as much variance in the trait as is expected
294 under a Brownian model of evolution.

295 Overfitting occurs when a model becomes overly complex by including too many
296 parameters (Everitt and Skrondal 2010). An overfitted model will perform well in explaining
297 initial data (training) but will perform poorly with new data or predictions (testing). The key to
298 preventing overfitting lies in optimising the choice of parameters to include in the model in
299 order to minimise test error. We chose the percentage of correct classification (PCC) obtained
300 through leave-one-out cross-validation (CV; Stone 1974) as our selection criterion. The higher
301 the PCC, the better the model performed under test conditions. Prior to performing CV
302 procedures, we generated a dissimilarity matrix from the correlation coefficients of the
303 geometric and microanatomical parameters before performing a hierarchical cluster analysis to
304 identify and eliminate highly correlated variables (correlation coefficient > 0.95) in order to
305 avoid subsequent complications related to the existence of singular variance-covariance
306 matrices. Pe_{min} , BCSA, TCSA and Z_{pol} were all inter-correlated. We decided to keep only the
307 parameter Pe_{min} which, in a paleobiological inference context, is the easiest to measure and least
308 likely to be impacted by taphonomy. The parameters P and RP were also correlated. We kept
309 the former and removed the latter from our data set. CV was performed with all possible
310 combinations of the remaining parameters (Pe_{min} , Ecc, SR, C_{obs} , P, S, RS, RPSD and RSSD)
311 and for each of the 100 phylogenetic trees for a total of more than 50,000 CV. In the end, only
312 three parameters out of the original 13 were retained for our humerus inference model (Pe_{min} ,
313 SR and P). The R script and associated R environment allowing to replicate the postural
314 inferences presented in the results of this study and allowing new inferences to be produced in
315 other extinct synapsids from our dataset are available in Online Resources 3 and 4, respectively.

316 We then designed linear models in R to examine the association of the coordinates of
317 the sampled taxa on the first and second axis of the PFDA model with body mass and lifestyle.
318 When lifestyle was significant, we performed pairwise post-hoc tests with false discovery rate
319 (FDR) correction using the `emmeans_test` function in the R package `rstatix` (Alboukadel 2021).

320 **Results**

321 PHYLOGENETIC SIGNAL IN THE DATA

322 All geometric parameters except for cross-sectional eccentricity (Ecc) were significantly
323 associated with phylogeny (Table 2). For Pe_{min} , BCSA, TCSA and Z_{pol} , the K-statistic was
324 below 1, indicating that intra-clade variation is greater than inter-clade variation and suggesting
325 patterns of evolutionary convergence. However, K was close to 1 for the slenderness ratio (SR),
326 implying that the distribution of this trait on the phylogeny is consistent with what would be

327 expected under a Brownian model of evolution and therefore reflects a phylogenetic signal. S
 328 and RPSD were the only microanatomical parameters to be significantly associated with
 329 phylogeny (Table 2). K was lower than 1 in each case, highlighting convergences. Posture also
 330 contained a substantial phylogenetic signal (P -value < 0.01), with the delta-statistic ranging
 331 from 3.194 to 21.471 (mean = 11.982; see Table 2).

332 **Table 2** Phylogenetic signal in the data. Values reported in the table are means obtain from 100
 333 phylogenetic trees. The P -values for K (Blomberg et al. 2003) and delta (Borges et al. 2019)
 334 are obtained from 1000 and 100 randomisations, respectively. Minimum and maximum values
 335 obtained from our distribution of 100 phylogenetic trees are given in parentheses. All geometric
 336 and microanatomical parameters, except ratios, were log-transformed in R

Parameter	K-statistic	Delta-statistic	P -value
Pe_{min}	0.58 (0.506–0.706)		0.001** (0.001–0.003)
BCSA	0.616 (0.536–0.745)		0.001** (0.001–0.003)
TCSA	0.593 (0.517–0.72)		0.001** (0.001–0.002)
Ecc	0.185 (0.1–0.251)		0.403 (0.194–0.63)
Z_{pol}	0.611 (0.531–0.742)		0.001** (0.001–0.002)
SR	0.915 (0.796–1.069)		0.001** (0.001–0.001)
P	0.237 (0.15–0.298)		0.151 (0.051–0.334)
S	0.392 (0.339–0.472)		0.007** (0.002–0.017)
C_{obs}	0.169 (0.078–0.254)		0.52 (0.177–0.781)
RP	0.225 (0.144–0.279)		0.186 (0.092–0.359)
RS	0.272 (0.237–0.332)		0.059 (0.03–0.105)
RPSD	0.697 (0.586–0.813)		0.001** (0.001–0.003)
RSSD	0.234 (0.2–0.274)		0.159 (0.081–0.278)
Posture		11.982 (3.194–21.471)	< 0.001*** (< 0.001–0.01)

337

338 GEOMETRIC AND MICROANATOMICAL COMPARISON OF POSTURAL GROUPS

339 The microanatomical parameter S and the geometric parameters Pe_{min} , BCSA, TCSA, Z_{pol} and
 340 SR are all significantly associated with posture (Table 3). They were also always significantly
 341 related to body mass and never to lifestyle except for SR and S, which are significantly
 342 associated with both body mass and lifestyle. RPSD was significantly associated only with

343 **Table 3** Effect of posture, body mass and functional ecology/lifestyle on the humeral geometric
 344 and microanatomical parameters. Values reported are means obtained from 100 phylogenetic
 345 trees. Minimum and maximum values obtained from our distribution of 100 phylogenetic trees
 346 are given in parentheses. Body mass and all geometric and microanatomical parameters, except
 347 ratios, were log-transformed in R. Abbreviations: BM, body mass; LS, lifestyle; POS, posture

GLS model formula	Independent variables	Chi-square values	P-values
Pe_{min} ~ BM + LS + POS	POS	14.653 (10.196–18.37)	0.003** (< 0.001–0.017)
	BM	536.358 (366.969–653.646)	< 0.001***
	LS	3.311 (2.21–4.439)	0.35 (0.218–0.53)
BCSA ~ BM + LS + POS	POS	13.884 (12.008–15.852)	0.003** (0.001–0.007)
	BM	551.749 (509.506–597.076)	< 0.001***
	LS	4.869 (4.208–5.937)	0.184 (0.115–0.24)
TCSA ~ BM + LS + POS	POS	18.178 (13.67–22.052)	< 0.001*** (< 0.001–0.003)
	BM	645.451 (478.171–755.691)	< 0.001***
	LS	4.688 (3.44–6.266)	0.2 (0.099–0.329)
Ecc ~ BM + LS + POS	POS	0.55 (0.274–0.987)	0.907 (0.804–0.965)
	BM	0.02 (< 0.001–0.161)	0.912 (0.689–0.999)
	LS	3.645 (2.009–5.04)	0.311 (0.169–0.571)
Z_{pol} ~ BM + LS + POS	POS	20.982 (18.529–23.534)	< 0.001***
	BM	794.205 (735.737–861.524)	< 0.001***
	LS	7.175 (5.93–8.665)	0.069 (0.034–0.115)
SR ~ BM + LS + POS	POS	15.664 (13.844–17.459)	0.001** (0.001–0.003)
	BM	13.869 (11.131–16.525)	< 0.001*** (< 0.001–0.001)
	LS	8.718 (7.529–10.025)	0.034* (0.018–0.057)
P ~ BM + LS + POS	POS	1.071 (0.614–1.524)	0.784 (0.677–0.893)
	BM	0.088 (0.003–0.248)	0.778 (0.619–0.956)
	LS	1.318 (0.848–1.788)	0.725 (0.617–0.838)
S ~ BM + LS + POS	POS	12.697 (11.016–14.076)	0.006** (0.003–0.012)
	BM	7.031 (6.033–8.012)	0.008** (0.005–0.014)
	LS	11.017 (9.13–13.989)	0.013* (0.003–0.028)
C_{obs} ~ BM + LS + POS	POS	1.288 (0.51–2.173)	0.733 (0.537–0.917)

	BM	0.063 (0.002–0.183)	0.812 (0.668–0.961)
	LS	2.529 (1.128–4.161)	0.478 (0.245–0.77)
RP ~ BM + LS + POS	POS	1.404 (0.826–1.963)	0.705 (0.58–0.843)
	BM	0.025 (< 0.001–0.134)	0.895 (0.714–0.999)
	LS	2.234 (1.449–2.94)	0.527 (0.401–0.694)
RS ~ BM + LS + POS	POS	4.919 (4.157–6.171)	0.18 (0.104–0.245)
	BM	9.705 (8.243–11.851)	0.002** (0.001–0.004)
	LS	6.89 (5.721–8.036)	0.077 (0.045–0.126)
RPSD ~ BM + LS + POS	POS	5.334 (4.365–6.047)	0.151 (0.109–0.225)
	BM	1.048 (0.373–2.005)	0.317 (0.157–0.541)
	LS	9.671 (8.443–11.623)	0.022* (0.009–0.038)
RSSD ~ BM + LS + POS	POS	2.482 (2.011–3.219)	0.48 (0.359–0.57)
	BM	5.234 (4.379–6.227)	0.023* (0.013–0.036)
	LS	3.955 (3.268–4.565)	0.268 (0.207–0.352)

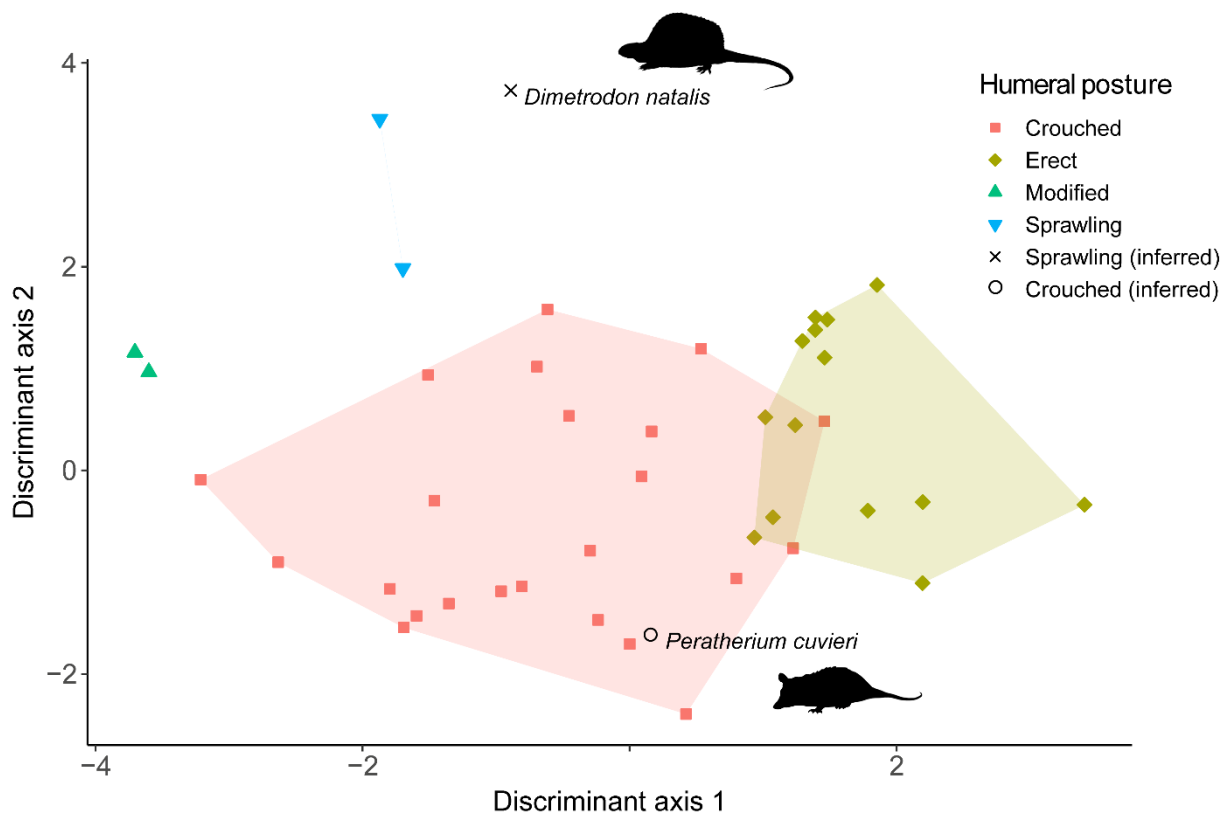
348

349 lifestyle, RS and RSSD only with body mass.

350 PHYLOGENETIC DISCRIMINATION OF POSTURAL GROUPS

351 The PFDA model was very successful in discriminating between postural groups (Fig. 4).
352 Indeed, the mean training PCC reached 88% (88-90%). Most of the time, crouched taxa were
353 correctly classified at 83% (19 out of 23 taxa). The rest of the time (5% of the phylogenetic
354 trees), they reached 87% (20 out of 23 taxa). With all tree hypotheses, the erect taxa were
355 correctly classified at 93% (13 out of 14 taxa) while the two monotremes (sprawling) and the
356 two talpids (modified) both achieved 100% of correct classifications. *Dimetrodon* and
357 *Peratherium* were always inferred as sprawling and crouched, respectively. Lambda ranged
358 from 0.04 to 0.17 (mean = 0.099), indicating a present but low influence of the phylogeny.

359 Body mass was significantly associated with the taxon coordinates on the first and
360 second PFDA axes (Table 4). Lifestyle was significantly associated with the taxon coordinates
361 on the first PFDA axis but not on the second, although the *P*-values were close to the
362 significance level. The results of the post-hoc tests with the first PFDA axis revealed that
363 arboreal taxa were significantly different from semi-aquatic, terrestrial and fossorial taxa, and
364 that fossorial taxa were significantly different from terrestrial taxa (Table 5).



365 **Fig. 4** Phylogenetic discriminant space generated from PFDA (Motani and Schmitz 2011) on
 366 postural groups. Based on posterior probabilities, *Dimetrodon* and *Peratherium* are inferred as
 367 “sprawling” and “crouched”, respectively. Silhouettes come from phylopic.org

368 Discussion

369 CROSS-SECTIONAL CHARACTERISATION OF POSTURAL GROUPS

370 Pe_{min} , BCSA, TCSA were all significantly associated with posture (Table 3). This is not
 371 surprising since Pe_{min} is related to body mass (Campione and Evans 2012), and it is well known
 372 that body mass and limb posture in mammals are related (Biewener 1989b, 2005; Houssaye et
 373 al. 2016b). Indeed, large mammals tend to have more erect (columnar) limbs that help reduce
 374 tissue stress (Gregory 1912; Biewener 1989a, Gatesy and Biewener 1991; Hutchinson 2021).
 375 This is because bone resists compression better than tension or torsion (Currey 2013).
 376 Logically, Pe_{min} increases with increasing bone size and so do both BCSA and TCSA. The
 377 significant association between Z_{pol} and posture is interesting, as it probably reveals a difference
 378 in torsional strength in the humerus between postures. Indeed, previous studies, including in-
 379 vivo measurements, have shown that crouched taxa, just like non-avian reptiles with a
 380 sprawling posture, exhibit increased torsional stress compared to erect taxa, which are primarily
 381 loaded in bending (Biewener 1990; Blob and Biewener 1999, 2001; Butcher et al. 2008, 2011).
 382 SR and S are the only parameters to be significantly associated with both posture and lifestyle.

383 **Table 4** Effect of body mass and lifestyle on the taxon coordinates on the first and second axes
 384 of the PFDA model. Values reported are means obtained from 100 phylogenetic trees.
 385 Minimum and maximum values obtained from our distribution of 100 phylogenetic trees are
 386 indicated in parentheses. Abbreviations: BM, body mass; LS, lifestyle

Linear model formula	Independent variable	F-value	P-value
Coordinates of the taxa on the first PFDA axis ~ BM + LS	BM	53.88 (46.071–57.117)	< 0.001***
	LS	11.807 (11.244–12.138)	< 0.001***
Coordinates of the taxa on the second PFDA axis ~ BM + LS	BM	14.499 (13.927–15.613)	< 0.001*** (< 0.001–0.001)
	LS	2.7 (2.526–2.767)	0.06 (0.056–0.073)

387

388 **Table 5** Differences in taxon coordinates on the first PFDA axis between lifestyle categories as
 389 shown by pairwise comparison. Values reported are means obtained from 100 phylogenetic
 390 trees. Minimum and maximum values obtained from our distribution of 100 phylogenetic trees
 391 are indicated in parentheses. Abbreviations: Aq, semi-aquatic; Ar, arboreal; Fo, fossorial; Te,
 392 terrestrial

Pairwise comparison	Adjusted P-value
Aq vs. Ar	0.006** (0.005–0.007)
Aq vs. Fo	0.547 (0.533–0.563)
Aq vs. Te	0.161 (0.145–0.171)
Ar vs. Fo	< 0.001***
Ar vs. Te	0.001** (< 0.001–0.001)
Fo vs. Te	0.028* (0.023–0.036)

393

394 Monotremes and talpids have some of the most robust humeri. These taxa are also the most
 395 fossorial species in our sample. This is because burrowing habits generally go hand in hand
 396 with robust, stocky forelimbs for digging in hard substrates (Shimer 1903). Similarly, the
 397 primates in our sample have the slenderest humeri. They are also the species with the most
 398 arboreal habits. Indeed, arboreal species generally have slender, elongated forelimbs that allow
 399 them to move more efficiently in trees by increasing reach and reducing energy expenditure
 400 during vertical climbing, as longer arms allow them to lean back more, thereby increasing
 401 friction between the foot and the substrate (Preuschoft et al. 1996; Isler 2005). The talpids show

402 the highest S values in the sample. Two reasons can explain these high S values: (1) The
403 presence of cancellous bone considerably extending the transition between the medulla and the
404 cortex. The corresponding compactness profile is flattened, resulting in a low slope of the
405 asymptote at point P and thus a high S value ($S = 1/\text{slope}$). (2) Heterogeneity of cortical
406 thickness. Variations in cortical thickness depending on the position within the cross-section
407 mimic an extensive transition between the medulla and the cortex on the overall compactness
408 profile. Talpids clearly show a thickening of the cortex antero-posteriorly (Fig. 2). An increase
409 in mechanical stress in these regions, due to the attachment of strong muscles involved in the
410 adduction/abduction cycle of the humerus (Rose et al. 2013), could explain these variations in
411 cortical thickness.

412 PHYLOGENETIC DISCRIMINANT MODEL AND PALAEOBIOLOGICAL INFERENCES

413 Lambda was always greater than 0, indicative of a phylogenetic involvement in the PFDA,
414 which attempts to maximise the relationships between humeral posture and the
415 microanatomical parameters. This result is far from being surprising. Indeed, we saw that
416 humeral posture was significantly associated with phylogeny (Table 2). Nevertheless, this
417 confirms our choice to use a classification method accounting for species relatedness. With a
418 mean correct classification rate exceeding 85%, the PFDA model was very successful in
419 discriminating the postural groups. Even monotremes and talpids, represented by only four
420 individual taxa (*Ornithorhynchus* and *Tachyglossus*, and *Euroscaptor* and *Talpa*, respectively),
421 are always correctly classified.

422 The Late Eocene herpetotheriid *Peratherium cuvieri* was inferred to be “crouched” with
423 all trees in our phylogenetic tree sample. Studies on herpetotheriid locomotion are very sparse.
424 Kurz (2005) designated *Amphiperatherium* and another undetermined herpetotheriid as
425 “cursorial” based on lumbar vertebral morphology and tail length. Horovitz et al. (2008)
426 described *Herpetotherium* as “agile” based on femoral morphology. The literature is more
427 abundant regarding their extant close relatives, the Didelphidae. The didelphids are commonly
428 used as models to study the evolution of therian locomotion (Jenkins 1971; Jenkins and Weijs
429 1979; Argot 2001; Butcher et al. 2011). Didelphids, like most small mammals, have a crouched
430 posture (Jenkins 1971). Thus, a crouched posture in *Peratherium cuvieri* is deemed very
431 plausible.

432 The posture of permo-carboniferous synapsids (the earliest stem mammals) has been
433 extensively studied, in comparison to that of herpetotheriids. Indeed, it is widely accepted,

434 based on anatomical, biomechanical, and ichnological evidence, that the earliest stem mammals
435 had sprawling limbs (Jenkins 1973; Hunt and Lucas 1998; Blob 2001; Benton 2015; Hopson
436 2015; Wright 2018; Cavanaugh 2021). Therefore, it is not surprising that *Dimetrodon natalis*
437 was inferred to be a sprawler by the PFDA model, although the postural has not yet been clearly
438 established. Sometimes described as “lizard-like” (Bakker 1971; Desmond 1975), the sprawling
439 posture of monotremes may in fact be close to the ancestral condition of synapsids, yet distinct
440 from the sprawling posture of squamates and urodeles (Gambaryan and Kuznetsov 2013;
441 Regnault et al. 2020), or it may be derived from early mammals with parasagittal limbs
442 (Pridmore 1985). Similarly in reptiles, Crocodylia, with their “semi-erect” limbs, were
443 commonly considered “primitive” posturally (Bakker 1971; Charig 1972), when in fact they
444 are descended from more erect forms (Parrish 1987; Gatesy 1991; Reilly and Elias 1998).

445 Body mass seems to have a confounding effect on our PFDA model (Table 4). This is
446 not surprising since the parameter $P_{e_{min}}$ was used in the model. We have already mentioned
447 that body mass and posture in mammals are strongly intertwined. But we do not see this as a
448 problem, on the contrary. Indeed, our goal is to build a model that can effectively discriminate
449 between humeral postures in mammals based on easily measurable parameters, including in
450 fossils, so that inferences can be produced for extinct taxa. If body mass is a powerful parameter
451 to achieve this goal, we should use it by including, or rather not excluding, parameters
452 associated with it, such as the perimeter of the cross-section. However, body mass, although
453 useful, is not sufficient to distinguish between postures. Indeed, some species have equivalent
454 body mass but different posture; e.g. *Marmota* (crouched) and *Tachyglossus* (sprawling). It
455 should also be mentioned here that some ungulates with erect limbs weigh less than 10 kg, e.g.
456 dik-diks (genus *Madoqua*). The case of small ungulates, although beyond the scope of this
457 study, is worthy of further investigation. Therefore, we believe that femoral geometric and
458 microanatomical parameters contain a functional signal that a multivariate quantitative
459 approach such as PFDA can effectively exploit. Lifestyle was significantly associated with the
460 first axis of the model and was close to the significance level for the second axis. This is most
461 likely due to the presence of SR in the model. Indeed, we saw that the slenderness ratio was
462 significantly associated with both body mass, posture, and lifestyle.

463 Post-hoc tests revealed that virtually all lifestyle categories were significantly different
464 on the first axis with the exception of semi-aquatic taxa (Table 5). However, the only semi-
465 aquatic taxon in our analysis was *Ornithorhynchus*. Therefore, this is most likely due to the
466 small sample size, which results in a lack of statistical power. However, semi-aquatic taxa, such

467 as otters, deserve a separate study, as they tend to show pachyostosis and/or osteosclerosis (an
468 increase in periosteal bone deposits and widespread spongiosa, respectively), which affect
469 buoyancy (Houssaye et al. 2016a).

470 At first glance, it is surprising that S was not retained in the PFDA model since it seems
471 to be significantly associated with posture unlike P (Table 3). However, the result of the cross-
472 validation with the parameters Pe_{min} , SR and S gives only 73% of correct classification (15%
473 less compared to the original model). Ultimately, joint use of Pe_{min} , SR and P seems to be the
474 best parameter configuration to discriminate mammalian posture with our sample.

475 **Conclusion**

476 Using generalised least squares, we showed that all parameters that were significantly
477 associated with posture, i.e. minimum humeral shaft perimeter (Pe_{min}), bone cross-sectional
478 area (BCSA), total cross-sectional area (TCSA), polar section modulus (Z_{pol}), slenderness ratio
479 (SR) and the reciprocal of the slope of the asymptote at point P on the compactness profile (S),
480 were also significantly associated with body mass. This was expected as body mass is known
481 to have an impact on posture in mammals, with smaller species having a crouched posture and
482 larger species having more erect limbs to minimise body weight-induced stresses. The
483 association between Z_{pol} and posture was also expected since Z_{pol} corresponds to the resistance
484 of the shaft to torsion, and previous studies have shown that in mammals (and other taxa)
485 crouched limbs are subject to higher torsional stresses than erect limbs, which are primarily
486 loaded in flexion. We showed that SR and S were also related to lifestyle, with burrowing taxa
487 having more robust humeri and arboreal taxa having slender humeri, and moles exhibiting
488 heterogeneity in cortical thickness most likely related to the attachment of strong muscles on
489 the anterior and posterior surfaces of the humerus involved in the limb adduction/abduction
490 cycle.

491 A number of parameters were significantly associated with phylogeny (Pe_{min} , BSCA,
492 TCSA, Z_{pol} , S and RPSD), as well as posture itself. The lambda values from the PFDA model
493 indicated an influence of the phylogeny in the data, justifying the use of a phylogenetically
494 informed classification method. Elimination of overly correlated parameters followed by cross-
495 validation procedures ultimately yielded a PFDA model with three variables (Pe_{min} , SR and P)
496 that successfully discriminated postural groups (88% average correct classification into four
497 categories based on 100 mammalian phylogenetic trees). Despite the small sample size, the
498 model was able to correctly classify moles (modified humeral posture) and monotremes

499 (sprawling humeral posture). Application of the model to extinct taxa yielded plausible results.
500 *Peratherium cuvieri* and *Dimetrodon natalis* are inferred to have had a crouched and sprawling
501 humeral posture, respectively. The PFDA model appeared to be significantly influenced by
502 body mass and lifestyle, but nevertheless allows quantitative postural discrimination that size
503 or lifestyle parameters alone would not achieve, while producing plausible inferences in extinct
504 taxa.

505 Our study highlights the complex interplay between body mass, lifestyle, posture and
506 the geometry and microanatomy of the humerus in mammals. Our model can be used by
507 palaeontologists to infer the humeral posture of other extinct species based on humeral cross-
508 sections alone. Extending our method to other appendicular skeletal elements could refine the
509 inferences produced for extinct taxa, particularly those relevant to the context of shifts in limb
510 posture (more sprawling to more erect/parasagittal limbs) in early mammals, which tend to
511 exhibit a mosaic of characters.

512 *Supplementary information*—The online version contains supplementary material available at
513 <https://doi.org/10.1007/s10914-023-09652-w>.

514 *Acknowledgements*—We warmly thank Alexandra Houssaye, Charlène Selva, Sandrine
515 Ladevèze and Guillaume Billet for sharing with us the CT data of some of the studied
516 specimens. We thank Joséphine Lesur, Géraldine Veron, Jacques Cuisin and Violaine Nicolas-
517 Colin for granting us access to the MNHN collections. We are grateful to Renaud Lebrun and
518 the MRI platform of the Université de Montpellier and to Marta Bellato and the AST-RX
519 platform of the MNHN for their help in collecting CT data. We are indebted to Margot Michaud
520 and Laura Bento Da Costa for their valuable advice and to Mathilde Aladini for her kind review
521 of the manuscript. We are grateful to our two anonymous reviewers, whose comments helped
522 to improve the quality of this study. We thank the Virtual Data initiative, run by the LabEx
523 P2IO and supported by the Université Paris-Saclay, for providing computing resources on its
524 cloud infrastructure.

525 *Author contributions*—JG collected the data, designed the study, performed the analyses,
526 interpreted the results, wrote the manuscript. JB designed the analyses. MG designed the
527 analyses. JRH interpreted the results. ML collected the data, designed the study, interpreted the
528 results. All authors reviewed and approved the final manuscript.

529 *Funding*—This work was supported by the doctoral programme Interfaces pour le vivant (IPV),
530 with the cooperation of Sorbonne Université, and by the ATM MNHN 2014 “formes possibles,
531 formes réalisées”.

532 *Data availability*—The data that support the findings of this study are included in this published
533 article and its online resources.

534 *Conflict of interest*—The authors declare that they have no conflicts of interest.

535 **References**

536 Abbott CP (2019) The *Dimetrodon* dilemma: reassessing posture in sphenacodontians and
537 related non-mammalian synapsids. Undergraduate honors dissertation, College of
538 William and Mary

539 Abràmoff MD, Magalhães PJ, Ram SJ (2004) Image processing with ImageJ. *Biophotonics Int*
540 11:36–42

541 Alboukadel K (2021) rstatix: pipe-friendly framework for basic statistical tests. R package
542 version 0.7.0

543 Amson E, Kolb C (2016) Scaling effect on the mid-diaphysis properties of long bones—the
544 case of the Cervidae (deer). *Sci Nat* 103:1–10. [https://doi.org/10.1007/s00114-016-](https://doi.org/10.1007/s00114-016-1379-7)
545 1379-7

546 Amson E, de Muizon C, Laurin M, Argot C, de Buffrénil V (2014) Gradual adaptation of bone
547 structure to aquatic lifestyle in extinct sloths from Peru. *Proc R Soc Lond B Biol Sci*
548 281:20140192. <https://doi.org/10.1098/rspb.2014.0192>

549 Argot C (2001) Functional-adaptive anatomy of the forelimb in the Didelphidae, and the
550 paleobiology of the Paleocene marsupials *Mayulestes ferox* and *Pucadelphys andinus*. *J*
551 *Morphol* 247:51–79. [https://doi.org/10.1002/1097-4687\(200101\)247:1<51::AID-](https://doi.org/10.1002/1097-4687(200101)247:1<51::AID-JMOR1003>3.0.CO;2-%23)
552 *JMOR1003*>3.0.CO;2-%23

553 Bakker RT (1971) Dinosaur physiology and the origin of mammals. *Evolution* 25:636–658.
554 <https://doi.org/10.1111/j.1558-5646.1971.tb01922.x>

555 Beck TJ, Ruff CB, Mourtada FA, Shaffer RA, Maxwell-Williams K, Kao GL, Sartoris DJ,
556 Brodine S (1996) Dual-energy X-ray absorptiometry derived structural geometry for

557 stress fracture prediction in male U.S. marine corps recruits. *J Bone Miner Res* 11:645–
558 653. <https://doi.org/10.1002/jbmr.5650110512>

559 Benton MJ (2015) *Vertebrate Palaeontology*. Wiley, Hoboken

560 Biewener AA (1989a) Mammalian terrestrial locomotion and size. *Bioscience* 39:776–783.
561 <https://doi.org/10.2307/1311183>

562 Biewener AA (1989b) Scaling body support in mammals: limb posture and muscle mechanics.
563 *Science* 245:45–48. <https://doi.org/10.1126/science.2740914>

564 Biewener AA (1990) Biomechanics of mammalian terrestrial locomotion. *Science* 250:1097–
565 1103. <https://doi.org/10.1126/science.2251499>

566 Biewener AA (2005) Biomechanical consequences of scaling. *J Exp Biol* 208:1665–1676.
567 <https://doi.org/10.1242/jeb.01520>

568 Bishop PJ, Hocknull SA, Clemente CJ, Hutchinson JR, Barrett RS, Lloyd DG (2018a)
569 Cancellous bone and theropod dinosaur locomotion. Part II—a new approach to
570 inferring posture and locomotor biomechanics in extinct tetrapod vertebrates. *PeerJ*
571 6:e5779. <https://doi.org/10.7717/peerj.5779>

572 Bishop PJ, Hocknull SA, Clemente CJ, Hutchinson JR, Farke AA, Barrett RS, Lloyd DG
573 (2018b) Cancellous bone and theropod dinosaur locomotion. Part III—inferring posture
574 and locomotor biomechanics in extinct theropods, and its evolution on the line to birds.
575 *PeerJ* 6:e5777. <https://doi.org/10.7717/peerj.5777>

576 Bishop PJ, Hocknull SA, Clemente CJ, Hutchinson JR, Farke AA, Beck BR, Barrett RS, Lloyd
577 DG (2018c) Cancellous bone and theropod dinosaur locomotion. Part I—an
578 examination of cancellous bone architecture in the hindlimb bones of theropods. *PeerJ*
579 6:e5778. <https://doi.org/10.7717/peerj.5778>

580 Blob RW (2000) Interspecific scaling of the hindlimb skeleton in lizards, crocodylians, felids
581 and canids: does limb bone shape correlate with limb posture? *J Zool* 250:507–531.
582 <https://doi.org/10.1111/j.1469-7998.2000.tb00793.x>

583 Blob RW (2001) Evolution of hindlimb posture in nonmammalian therapsids: biomechanical
584 tests of paleontological hypotheses. *Paleobiology* 27:14–38.
585 [https://doi.org/10.1666/0094-8373\(2001\)0272.0.CO;2](https://doi.org/10.1666/0094-8373(2001)0272.0.CO;2)

- 586 Blob RW, Biewener AA (1999) In vivo locomotor strain in the hindlimb bones of *Alligator*
587 *mississippiensis* and *Iguana iguana*: implications for the evolution of limb bone safety
588 factor and non-sprawling limb posture. *J Exp Biol* 202:1023–1046.
589 <https://doi.org/10.1242/jeb.202.9.1023>
- 590 Blob RW, Biewener AA (2001) Mechanics of limb bone loading during terrestrial locomotion
591 in the green iguana (*Iguana iguana*) and American alligator (*Alligator mississippiensis*).
592 *J Exp Biol* 204:1099–1122. <https://doi.org/10.1242/jeb.204.6.1099>
- 593 Blomberg SP, Garland T, Ives AR (2003) Testing for phylogenetic signal in comparative data:
594 behavioral traits are more labile. *Evolution* 57:717–745. [https://doi.org/10.1111/j.0014-](https://doi.org/10.1111/j.0014-3820.2003.tb00285.x)
595 [3820.2003.tb00285.x](https://doi.org/10.1111/j.0014-3820.2003.tb00285.x)
- 596 Borges R, Machado JP, Gomes C, Rocha AP, Antunes A (2019) Measuring phylogenetic signal
597 between categorical traits and phylogenies. *Bioinformatics* 35:1862–1869.
598 <https://doi.org/10.1093/bioinformatics/bty800>
- 599 Brocklehurst N, Kammerer CF, Fröbisch J (2013) The early evolution of synapsids, and the
600 influence of sampling on their fossil record. *Paleobiology* 39:470–490.
601 <https://doi.org/10.1666/12049>
- 602 Brocklehurst RJ, Fahn-Lai P, Regnault S, Pierce SE (2022) Musculoskeletal modeling of
603 sprawling and parasagittal forelimbs provides insight into synapsid postural transition.
604 *iScience* 25:103578. <https://doi.org/10.1016/j.isci.2021.103578>
- 605 Butcher MT, Espinoza NR, Cirilo SR, Blob RW (2008) In vivo strains in the femur of river
606 cooter turtles (*Pseudemys concinna*) during terrestrial locomotion: tests of force-
607 platform models of loading mechanics. *J Exp Biol* 211:2397–2407.
608 <https://doi.org/10.1242/jeb.018986>
- 609 Butcher MT, White BJ, Hudzik NB, Gosnell WC, Parrish JH, Blob RW (2011) In vivo strains
610 in the femur of the Virginia opossum (*Didelphis virginiana*) during terrestrial
611 locomotion: testing hypotheses of evolutionary shifts in mammalian bone loading and
612 design. *J Exp Biol* 214:2631–2640. <https://doi.org/10.1242/jeb.049544>
- 613 Campione NE, Evans DC (2012) A universal scaling relationship between body mass and
614 proximal limb bone dimensions in quadrupedal terrestrial tetrapods. *BMC Biol* 10:1–
615 22. <https://doi.org/10.1186/1741-7007-10-60>

- 616 Canoville A, Laurin M (2009) Microanatomical diversity of the humerus and lifestyle in
617 lissamphibians. *Acta Zool* 90:110–122. [https://doi.org/10.1111/j.1463-](https://doi.org/10.1111/j.1463-6395.2008.00328.x)
618 [6395.2008.00328.x](https://doi.org/10.1111/j.1463-6395.2008.00328.x)
- 619 Canoville A, Laurin M (2010) Evolution of humeral microanatomy and lifestyle in amniotes,
620 and some comments on palaeobiological inferences. *Biol J Linn Soc Lond* 100:384–
621 406. <https://doi.org/10.1111/j.1095-8312.2010.01431.x>
- 622 Canoville A, de Buffrénil V, Laurin M (2021) Bone microanatomy and lifestyle in tetrapods.
623 In: de Buffrénil V, de Ricqlès AJ, Zylberberg L, Padian K, Laurin M, Quilhac A (eds)
624 *Vertebrate Skeletal Histology and Paleohistology*. CRC Press, Boca Raton, pp 724–743
- 625 Carrano MT (1999) What, if anything, is a cursor? Categories versus continua for determining
626 locomotor habit in mammals and dinosaurs. *J Zool* 247:29–42.
627 <https://doi.org/10.1111/j.1469-7998.1999.tb00190.x>
- 628 Cavanaugh T (2021) Reconstructing body size and center of mass in synapsids. Dissertation,
629 Harvard University
- 630 Charig AJ (1972) The evolution of the archosaur pelvis and hindlimb: an explanation in
631 functional terms. In: Joysey KA, Kemp TS (eds) *Studies in Vertebrate Evolution*. Oliver
632 and Boyd, Edinburgh, pp 121–155
- 633 Cooper LN, Clementz MT, Usip S, Bajpai S, Hussain ST, Hieronymus TL (2016) Aquatic
634 habits of cetacean ancestors: integrating bone microanatomy and stable isotopes. *Integr*
635 *Comp Biol* 56:1370–1384. <https://doi.org/10.1093/icb/icw119>
- 636 Currey JD (2013) *Bones: Structure and Mechanics*. Princeton University Press, Princeton.
637 <https://doi.org/10.1515/9781400849505>
- 638 D’Août K, Vereecke EE, Schoonaert K, De Clercq D, Van Elsacker L, Aerts P (2004)
639 Locomotion in bonobos (*Pan paniscus*): differences and similarities between bipedal
640 and quadrupedal terrestrial walking, and a comparison with other locomotor modes. *J*
641 *Anat* 204:353–361. <https://doi.org/10.1111/j.0021-8782.2004.00292.x>
- 642 Debuysschere M (2015) Origine et première diversification des mammaliaformes : apport des
643 faunes du Trias supérieur de Lorraine, France. Dissertation, Muséum national d’Histoire
644 naturelle, Paris Desmond AJ (1975) *The Hot-Blooded Dinosaurs*. Blond and Briggs,
645 London

646 Didier G, Laurin M (2020) Exact distribution of divergence times from fossil ages and tree
647 topologies. *Syst Biol* 69:1068–1087. <https://doi.org/10.1093/sysbio/syaa021>

648 Doube M, Klosowski MM, Arganda-Carreras I, Cordelières FP, Dougherty RP, Jackson JS,
649 Schmid B, Hutchinson JR, Shefelbine SJ (2010) BoneJ: free and extensible bone image
650 analysis in ImageJ. *Bone* 47:1076–1079. <https://doi.org/10.1016/j.bone.2010.08.023>

651 Everitt BS, Skrondal A (2010) *The Cambridge Dictionary of Statistics*. Cambridge University
652 Press, Cambridge

653 Fabbri M, Navalón G, Benson RBJ, Pol D, O’Connor J, Bhullar BAS, Erickson GM, Norell
654 MA, Orkney A, Lamanna MC, Zouhri S, Becker J, Emke A, Dal Sasso C, Bindellini G,
655 Maganuco S, Auditore M, Ibrahim N (2022) Subaqueous foraging among carnivorous
656 dinosaurs. *Nature* 603:1–6. <https://doi.org/10.1038/s41586-022-04528-0>

657 Gambaryan PP, Kielan-Jaworowska Z (1997) Sprawling versus parasagittal stance in
658 multituberculate mammals. *Acta Palaeontol Pol* 42:13–44

659 Gambaryan PP, Kuznetsov AN (2013) An evolutionary perspective on the walking gait of the
660 long-beaked echidna. *J Zool* 290:58–67. <https://doi.org/10.1111/jzo.12014>

661 Gatesy SM (1991) Hind limb movements of the American alligator (*Alligator mississippiensis*)
662 and postural grades. *J Zool* 224:577–588. <https://doi.org/10.1111/j.1469-7998.1991.tb03786.x>

664 Gatesy SM, Biewener AA (1991) Bipedal locomotion: effects of speed, size and limb posture
665 in birds and humans. *J Zool* 224:127–147. <https://doi.org/10.1111/j.1469-7998.1991.tb04794.x>

667 Gerkema MP, Davies WI, Foster RG, Menaker M, Hut RA (2013) The nocturnal bottleneck
668 and the evolution of activity patterns in mammals. *Proc R Soc Lond B Biol Sci*
669 280:20130508. <https://doi.org/10.1098/rspb.2013.0508>

670 Germain D, Laurin M (2005) Microanatomy of the radius and lifestyle in amniotes (Vertebrata,
671 Tetrapoda). *Zool Scr* 34:335–350. <https://doi.org/10.1111/j.1463-6409.2005.00198.x>

672 Gill PG, Purnell MA, Crumpton N, Brown KR, Gostling NJ, Stampanoni M, Rayfield EJ (2014)
673 Dietary specializations and diversity in feeding ecology of the earliest stem mammals.
674 *Nature* 512:303–305. <https://doi.org/10.1038/nature13622>

- 675 Girondot M, Laurin M (2003) Bone Profiler: a tool to quantify, model, and statistically compare
676 bone-section compactness profiles. *J Vertebr Paleontol* 23:458–461
- 677 Gônet J, Laurin M, Girondot M (2022) BoneProfileR: the next step to quantify, model and
678 statistically compare bone section compactness profiles. *Palaeontol Electron* 25:a12
679 <https://doi.org/10.26879/1194>
- 680 Gregory WK (1912) Notes on the principles of quadrupedal locomotion and on the mechanism
681 of the limbs in hoofed animals. *Ann N Y Acad Sci* 22:267–294.
682 <https://doi.org/10.1111/j.1749-6632.1912.tb55164.x>
- 683 Hastie T, Tibshirani R, Buja A (1994) Flexible discriminant analysis by optimal scoring. *J Am*
684 *Stat Assoc* 89:1255–1270. <https://doi.org/10.1080/01621459.1994.10476866>
- 685 Hopson JA (2015) Fossils, trackways, and transitions in locomotion: a case study of
686 *Dimetrodon*. In: Dial KP, Shubin N, Brainerd EL (eds) *Great Transformations in*
687 *Vertebrate Evolution*. University of Chicago Press, Chicago, pp 125–141
- 688 Horovitz I, Ladevèze S, Argot C, Macrini TE, Martin T, Hooker JJ, Kurz C, Muizon C de,
689 Sánchez-Villagra MR (2008) The anatomy of *Herpetotherium cf. fugax* Cope, 1873, a
690 metatherian from the Oligocene of North America. *Palaeontographica Abt A* 284:109–
691 141. <https://doi.org/10.1127/pala/284/2008/109>
- 692 Houssaye A, Botton-Divet L (2018) From land to water: evolutionary changes in long bone
693 microanatomy of otters (Mammalia: Mustelidae). *Biol J Linn Soc Lond* 125:240–249.
694 <https://doi.org/10.1093/biolinnean/bly118>
- 695 Houssaye A, Sander PM, Klein N (2016a) Adaptive patterns in aquatic amniote bone
696 microanatomy—more complex than previously thought. *Integr Comp Biol* 56:1349–
697 1369. <https://doi.org/10.1093/icb/icw120>
- 698 Houssaye A, Waskow K, Hayashi S, Cornette R, Lee AH, Hutchinson JR (2016b)
699 Biomechanical evolution of solid bones in large animals: a microanatomical
700 investigation. *Biol J Linn Soc Lond* 117:350–371. <https://doi.org/10.1111/bij.12660>
- 701 Houssaye A, Taverne M, Cornette R (2018) 3D quantitative comparative analysis of long bone
702 diaphysis variations in microanatomy and cross-sectional geometry. *J Anat* 232:836–
703 849. <https://doi.org/10.1111/joa.12783>

704 Hu Y, Meng J, Wang Y, Li C (2005) Large Mesozoic mammals fed on young dinosaurs. *Nature*
705 433:149–152. <https://doi.org/10.1038/nature03102>

706 Hunt AP, Lucas SG (1998) Vertebrate tracks and the myth of the belly-dragging, tail-dragging
707 tetrapods of the Late Paleozoic. *N M Mus Nat Hist Bull* 12:67–69

708 Hutchinson JR (2006) The evolution of locomotion in archosaurs. *C R Palevol* 5:519–530.
709 <https://doi.org/10.1016/j.crpv.2005.09.002>

710 Hutchinson JR (2021) The evolutionary biomechanics of locomotor function in giant land
711 animals. *J Exp Biol* 224:jeb217463. <https://doi.org/10.1242/jeb.217463>

712 Ibrahim N, Sereno PC, Dal Sasso C, Maganuco S, Fabbri M, Martill DM, Zouhri S, Myhrvold
713 NP, Iurino DA (2014) Semiaquatic adaptations in a giant predatory dinosaur. *Science*
714 345:1613–1616. <https://doi.org/10.1126/science.1258750>

715 Isler K (2005) 3D-kinematics of vertical climbing in hominoids. *Am J Phys Anthropol*
716 126:6681. <https://doi.org/10.1002/ajpa.10419>

717 Jenkins FA (1971) Limb posture and locomotion in the Virginia opossum (*Didelphis*
718 *marsupialis*) and in other non-cursorial mammals. *J Zool* 165:303–315.
719 <https://doi.org/10.1111/j.1469-7998.1971.tb02189.x>

720 Jenkins FA (1973) The functional anatomy and evolution of the mammalian humero-ulnar
721 articulation. *Am J Anat* 137:281–297. <https://doi.org/10.1002/aja.1001370304>

722 Jenkins FA, Parrington FR (1976) The postcranial skeletons of the Triassic mammals
723 *Eozostrodon*, *Megazostrodon* and *Erythrotherium*. *Philos Trans R Soc Lond B Biol Sci*
724 273:387–431. <https://doi.org/10.1098/rstb.1976.0022>

725 Jenkins FA, Weijs WA (1979) The functional anatomy of the shoulder in the Virginia opossum
726 (*Didelphis virginiana*). *J Zool* 188:379–410. <https://doi.org/10.1111/j.1469-7998.1979.tb03423.x>

728 Jones KE, Dickson BV, Angielczyk KD, Pierce SE (2021) Adaptive landscapes challenge the
729 “lateral-to-sagittal” paradigm for mammalian vertebral evolution. *Curr Biol*
730 31:18831892. <https://doi.org/10.1016/j.cub.2021.02.009>

731 Kemp TS (2005) *The Origin and Evolution of Mammals*. Oxford University Press, Oxford.
732 <https://doi.org/10.1093/oso/9780198507604.001.0001>

- 733 Kielan-Jaworowska Z, Hurum JH (2006) Limb posture in early mammals: sprawling or
734 parasagittal. *Acta Palaeontol Pol* 51:393–406
- 735 Kielan-Jaworowska Z, Cifelli RL, Luo Z-X (2004) *Mammals from the Age of Dinosaurs:
736 Origins, Evolution, and Structure*. Columbia University Press, New York
- 737 Kilbourne B, Hutchinson JR (2019) Morphological diversification of biomechanical traits:
738 mustelid locomotor specializations and the macroevolution of long bone cross-sectional
739 morphology. *BMC Evol Biol* 19:37. <https://doi.org/10.1186/s12862-019-1349-8>
- 740 Klein N, Sander PM, Krahl A, Scheyer TM, Houssaye A (2016) Diverse aquatic adaptations in
741 *Nothosaurus* spp. (Sauropterygia)—inferences from humeral histology and
742 microanatomy. *PLoS One* 11:e0158448. <https://doi.org/10.1371/journal.pone.0158448>
- 743 Krilloff A, Germain D, Canoville A, Vincent P, Sache M, Laurin M (2008) Evolution of bone
744 microanatomy of the tetrapod tibia and its use in palaeobiological inference. *J Evol Biol*
745 21:807–826. <https://doi.org/10.1111/j.1420-9101.2008.01512.x>
- 746 Kurz C (2005) Ecomorphology of opossum-like marsupials from the Tertiary of Europe and a
747 comparison with selected taxa. *Kaupia* 14:21–26
- 748 Laurin M, Canoville A, Germain D (2011) Bone microanatomy and lifestyle: a descriptive
749 approach. *C R Palevol* 10:381–402. <https://doi.org/10.1016/j.crpv.2011.02.003>
- 750 Lebrun R (2018) MorphoDig, an open-source 3D freeware dedicated to biology. *IPC5 Abstract
751 Book*:399
- 752 Lin Y-F, Konow N, Dumont ER (2019) How moles walk; it's all thumbs. *Biol Lett*
753 15:20190503. <https://doi.org/10.1098/rsbl.2019.0503>
- 754 Main RP, Simons EL, Lee AH (2021) Interpreting mechanical function in extant and fossil long
755 bones. In: de Buffrénil V, de Ricqlès AJ, Zylberberg L, Padian K, Laurin M, Quilhac A
756 (eds) *Vertebrate Skeletal Histology and Paleohistology*. CRC Press, Boca Raton, pp
757 688–723
- 758 Meier PS, Bickelmann C, Scheyer TM, Koyabu D, Sánchez-Villagra MR (2013) Evolution of
759 bone compactness in extant and extinct moles (Talpidae): exploring humeral
760 microstructure in small fossorial mammals. *BMC Evol Biol* 13:110.
761 <https://doi.org/10.1186/1471-2148-13-55>

- 762 Meng J (2014) Mesozoic mammals of China: implications for phylogeny and early evolution
763 of mammals. *Natl Sci Rev* 1:521542. <https://doi.org/10.1093/nsr/nwu070>
- 764 Motani R, Schmitz L (2011) Phylogenetic versus functional signals in the evolution of form–
765 function relationships in terrestrial vision. *Evolution* 65:2245–2257.
766 <https://doi.org/10.1111/j.1558-5646.2011.01271.x>
- 767 Myhrvold NP, Baldrige E, Chan B, Sivam D, Freeman DL, Ernest SKM (2015) An amniote
768 life-history database to perform comparative analyses with birds, mammals, and
769 reptiles. *Ecology* 96:3109–3109. <https://doi.org/10.1890/15-0846R.1>
- 770 Nakajima Y, Hirayama R, Endo H (2014) Turtle humeral microanatomy and its relationship to
771 lifestyle. *Biol J Linn Soc Lond* 112:719–734. <https://doi.org/10.1111/bij.12336>
- 772 Niemitz C (2010) The evolution of the upright posture and gait—a review and a new synthesis.
773 *Naturwissenschaften* 97:241–263. <https://doi.org/10.1007/s00114-009-0637-3>
- 774 Pagel M (1999) Inferring the historical patterns of biological evolution.
775 *Nature* 401:877–884. <https://doi.org/10.1038/44766>
- 776 Parrish JM (1987) The origin of crocodylian locomotion. *Paleobiology* 13:396–414.
777 <https://doi.org/10.1017/S0094837300009003>
- 778 Pietersen DW, Jansen R, Swart J, Panaino W, Kotze A, Rankin P, Nebe B (2020) Temminck’s
779 pangolin *Smutsia temminckii* (Smuts, 1832). In: Challender DWS, Nash HC, Waterman
780 C (eds) *Pangolins: Science, Society and Conservation*. Elsevier, Amsterdam, pp 175–
781 193. <https://doi.org/10.1016/B978-0-12-815507-3.00011-3>
- 782 Pinheiro J, Bates D, DebRoy S, Sarkar D, R Core Team (2021) nlme: linear and nonlinear
783 mixed effects. R package version 3.1–153
- 784 Plasse M, Amson E, Bardin J, Grimal Q, Germain D (2019) Trabecular architecture in the
785 humeral metaphyses of non-avian reptiles (Crocodylia, Squamata and Testudines):
786 lifestyle, allometry and phylogeny. *J Morphol* 280:982–998.
787 <https://doi.org/10.1002/jmor.20996>
- 788 Preuschoft H, Witte H, Christian A, Fischer M (1996) Size influences on primate locomotion
789 and body shape, with special emphasis on the locomotion of ‘small mammals’. *Folia*
790 *Primatol* 66:93112. <https://doi.org/10.1159/000157188>

791 Pridmore PA (1985) Terrestrial locomotion in monotremes (Mammalia: Monotremata). *J Zool*
792 205:53–73. <https://doi.org/10.1111/j.1469-7998.1985.tb05613.x>

793 Quemeneur S, de Buffrénil V, Laurin M (2013) Microanatomy of the amniote femur and
794 inference of lifestyle in limbed vertebrates. *Biol J Linn Soc Lond* 109:644–655.
795 <https://doi.org/10.1111/bij.12066>

796 R Core Team (2013) R: a language and environment for statistical computing. R Foundation
797 for Statistical Computing, Vienna

798 Regnault S, Fahn-Lai P, Norris RM, Pierce SE (2020) Shoulder muscle architecture in the
799 echidna (Monotremata: *Tachyglossus aculeatus*) indicates conserved functional
800 properties. *J Mamm Evol* 27:591–603. <https://doi.org/10.1007/s10914-020-09498-6>

801 Reilly SM, Elias JA (1998) Locomotion in *Alligator mississippiensis*: kinematic effects of
802 speed and posture and their relevance to the sprawling-to-erect paradigm. *J Exp Biol*
803 201:2559–2574. <https://doi.org/10.1242/jeb.201.18.2559>

804 Revell LJ (2012) phytools: an R package for phylogenetic comparative biology (and other
805 things). *Methods Ecol Evol* 3:217–223. [https://doi.org/10.1111/j.2041-](https://doi.org/10.1111/j.2041-210X.2011.00169.x)
806 [210X.2011.00169.x](https://doi.org/10.1111/j.2041-210X.2011.00169.x)

807 Rose KD (2006) *The Beginning of the Age of Mammals*. Johns Hopkins University Press,
808 Baltimore

809 Rose JA, Sandefur M, Huskey S, Demler JL, Butcher MT (2013) Muscle architecture and out-
810 force potential of the thoracic limb in the eastern mole (*Scalopus aquaticus*). *J Morphol*
811 274:1277–1287. <https://doi.org/10.1002/jmor.20178>

812 Russo GA, Kirk EC (2017) Another look at the foramen magnum in bipedal mammals. *J Hum*
813 *Evol* 105:24–40. <https://doi.org/10.1016/j.jhevol.2017.01.018>

814 Scheidt A, Wölfer J, Nyakatura JA (2019) The evolution of femoral cross-sectional properties
815 in sciuriform rodents: influence of body mass and locomotor ecology. *J Morphol*
816 280:11561169. <https://doi.org/10.1002/jmor.21007>

817 Seilacher A (1970) Arbeitskonzept zur Konstruktions-Morphologie. *Lethaia* 3:393–396.
818 <https://doi.org/10.1111/j.1502-3931.1970.tb00830.x>

- 819 Selva C (2017) Morphologie et fonction du système vestibulaire de l'oreille interne des
820 mammifères souterrains. Dissertation, Muséum national d'Histoire naturelle, Paris
- 821 Sereno PC (2006) Shoulder girdle and forelimb in multituberculates: evolution of parasagittal
822 forelimb posture in mammals. In: Carrano MT, Gaudin TJ, Blob RW, Wible JR (eds)
823 Amniote Paleobiology: Perspectives on the Evolution of Mammals, Birds, and Reptiles.
824 University of Chicago Press, Chicago, pp 315–366
- 825 Shannon CE (1948) A mathematical theory of communication. *Bell Sys Tech J* 27:379–423.
826 <https://doi.org/10.1002/j.1538-7305.1948.tb01338.x>
- 827 Shimer HW (1903) Adaptations to aquatic, arboreal, fossorial and cursorial habits in mammals.
828 III. Fossorial adaptations. *Am Nat* 37:819–825. <https://doi.org/10.1086/278368>
- 829 Stadler T (2011) Mammalian phylogeny reveals recent diversification rate shifts. *Proc Natl*
830 *Acad Sci U S A* 108:6187–6192. <https://doi.org/10.1073/pnas.1016876108>
- 831 Stein BR, Casinos A (1997) What is a cursorial mammal? *J Zool* 242:185–192.
832 <https://doi.org/10.1111/j.1469-7998.1997.tb02939.x>
- 833 Stone M (1974) Cross-validatory choice and assessment of statistical predictions. *J R Stat Soc*
834 *Series B Stat Methodol* 36:111133. [https://doi.org/10.1111/j.2517-](https://doi.org/10.1111/j.2517-6161.1974.tb00994.x)
835 [6161.1974.tb00994.x](https://doi.org/10.1111/j.2517-6161.1974.tb00994.x)
- 836 Tommasini SM, Nasser P, Schaffler MB, Jepsen KJ (2005) Relationship between bone
837 morphology and bone quality in male tibias: implications for stress fracture risk. *J Bone*
838 *Miner Res* 20:1372–1380. <https://doi.org/10.1359/JBMR.050326>
- 839 Upham NS, Esselstyn JA, Jetz W (2019) Inferring the mammal tree: species-level sets of
840 phylogenies for questions in ecology, evolution, and conservation. *PLoS Biol*
841 17:e3000494. <https://doi.org/10.1371/journal.pbio.3000494>
- 842 Vaughan TA, Ryan JM, Czaplewski NJ (2015) *Mammalogy*. Jones and Bartlett Learning,
843 Burlington
- 844 Wagstaffe AY, O'Driscoll AM, Kunz CJ, Rayfield EJ, Janis CM (2022) Divergent locomotor
845 evolution in “giant” kangaroos: evidence from foot bone bending resistances and
846 microanatomy. *J Morphol* 283:313–332. <https://doi.org/10.1002/jmor.21445>

- 847 Wilson GP, Evans AR, Corfe IJ, Smits PD, Fortelius M, Jernvall J (2012) Adaptive radiation
848 of multituberculate mammals before the extinction of dinosaurs. *Nature* 483:457–460.
849 <https://doi.org/10.1038/nature10880>
- 850 Wright M (2018) Functional morphology of the hindlimb during the transition from sprawling
851 to parasagittal gaits in synapsid evolution. Dissertation, Harvard University and
852 University of Groningen